CVD diamond detector with interdigitated electrode pattern for time-of-flight energy-loss measurements of low-energy ion bunches

W. Cayzac, Michal Pomorski, A. Blažević, B. Canaud, D. Deslandes, J. Fariaut, D. Gontier, E. Lescoute, J.G. Marmouget, F. Occelli, et al.

CVD diamond detector with interdigitated electrode pattern for time-of-flight energy-loss measurements of low-energy ion bunches

W. Cayzac,[1, a)] M. Pomorski,[2] B. Canaud,[1] D. Deslandes,[1] J. Fariaut,[1] D. Gontier,[1] E. Lescoute,[1] J. G. Marmouget,[1] F. Occelli,[1] G. Oudot,[1] C. Reverdin,[1] J. E. Sauvestre,[1] A. Sollier,[1] G. Soullié,[1] C. Varignon,[1] B. Villette,[1] and A. Blažević[3]

[1)] *CEA, DIF, F-91297 Arpajon, France*

[2)] *CEA-LIST, Diamond Sensors Laboratory, Gif-sur-Yvette F-91191, France*

[3)] *GSI Helmholtzzentrum für Schwerionenforschung, Planckstr.1, 64291 Darmstadt, Germany*

(Dated: 4 April 2018)

Ion stopping experiments in plasma for beam energies of few hundred keV per nucleon are of great interest to benchmark the stopping-power models in the context of inertial confinement fusion and high-energy-density physics research. For this purpose, a specific ion detector on chemical-vapor-deposition diamond basis has been developed for precise time-of-flight measurements of the ion energy loss. The electrode structure is interdigitated for maximizing its sensitivity to low-energy ions and it has a finger width of 100 µm and a spacing of 500 µm. A short single α-particle response is obtained, with signals as narrow as 700 ps at FWHM. The detector has been tested with α-particle bunches at a 500 keV per nucleon energy, showing an excellent time-of-flight resolution down to 20 ps. In this way, beam energy resolutions from 0.4 keV to a few keV have been obtained in an experimental configuration using a 100 µg/cm^2 thick carbon foil as energy-loss target and a 2 m time-of-flight distance. This allows a highly precise beam energy measurement of $\delta E/E \approx 0.04$–$0.2\,\%$ and a resolution on the energy loss of 0.6–2.5 % for a fine testing of stopping-power models.

The stopping power (dE/dx) of ions in ionized matter[1,2] is a central issue in high-energy density physics (HEDP)[3] and, foremost, in inertial confinement fusion (ICF)[4–8]. However, a systematic experimental database is still missing and precise measurements of the energy loss of ions in plasma are required in order to benchmark the theoretical stopping-power models. The largest differences between the stopping predictions of various models are reported near the stopping-power peak, for projectile velocities comparable to the velocity of the thermal electrons in plasma[1]. This maximum is of special importance as it gives rise to the Bragg peak of energy deposition in a given target, yet measurements in this parameter range are very scarce[9,10].

Experiments aimed at measuring the ion energy loss close to the stopping-power peak in plasma are considered at CEA-DIF on the 4MV Van-De-Graaff accelerator facility in combination with the GCLT (Générateur de Chocs Laser Transportable) laser system. In these experiments, a 100 µg/cm^2 thick carbon foil is heated by two laser beams to a hot and highly ionized plasma state. For the achievable plasma temperatures of few tens to few hundred eV relevant for ICF and HEDP, the stopping power for interacting projectile ions peaks at beam energies of few hundred keV per nucleon. Hence, the plasma is probed by a bunched beam of α-particles in this low energy range. The ion energy loss in plasma is measured using the time-of-flight (TOF) method. This requires a detector with excellent timing properties for precise TOF measurements, a sufficient radiation hardness to withstand an important ion flux, a sufficiently large detection area, and an optimized sensitivity to low-energy ions. Here, these conditions are fulfilled by a detector on chemical-vapor-deposition (CVD)-diamond basis.

CVD-produced diamond features remarkable properties in terms of radiation hardness, sensitivity, high time resolution and fast time response. These characteristics, associated with suited low-noise broadband electronics, make CVD-diamond an ideal material for both high-rate single particle counting and ion TOF applications[11,12]. This is why, during the past 20 years, CVD-diamond has been increasingly used for ion detection in particle accelerator facilities, in atomic, nuclear and HEDP experiments[13–17] as well as for beam monitoring and heavy ion dosimetry[18,19]. TOF resolutions in the order of 20–40 ps have been reported[13,14,16,17].

CVD-diamond detectors used in previous experiments on the energy loss of ions in plasma[10,20,21] are described or are similar to the ones presented in Ref.[22]. As in these latter works, the diamond film is here chosen to be polycrystalline. In contrast to single-crystal CVD diamond, polycrystalline CVD diamond is indeed available in larger areas and is more cost-effective. Nevertheless, it features a lower charge-collection efficiency (CCE) notably due to charge trapping at the grain boundaries[23,24].

The detectors used in previous experiments are based on a plane capacitor electrode (or "sandwich") geometry, with metalization on both sides of the diamond film. This configuration results in a uniform electric field across the sample and in a charge transport normal to the electrodes. It is therefore most suited to the detection of ions that have a range in diamond larger or similar to the

[a)] Current affiliation: Centre de Mathématiques et de Leurs Applications, ENS Cachan and CNRS, UniverSud, 61 Avenue du Président Wilson, F-94235 Cachan Cedex, France;
e-mail: cayzacwitold@gmail.com

film thickness. In this way, the ion energy deposition as well as the ionization density are uniform in the diamond volume, which leads to an optimized charge collection and time resolution. For example, in the energy-loss experiments of Ref.[20,21], the projectile ions have an energy of 4 MeV per nucleon and a range in diamond around 22 µm, and the diamond films are 20 µm thick[22]. In contrast, in Ref.[10], where the energy loss at the stopping-power peak is measured, the detected ions have a lower energy of 500–600 keV per nucleon. Then, the ion range in diamond is only about 3 µm, while the diamond thickness is 13 µm. In this case, polarization effects due to a non-uniform energy deposition in the sample are likely to generate a significant space charge that degrades the charge collection and, thus, the signal amplitude[25–28]. Therefore, even if the recorded bunch signals did permit a sufficiently precise energy-loss analysis, the time resolution of the measurements was not optimal for these low-energy ions using this detector geometry.

In order to ensure highly precise TOF measurements at projectile energies of a few hundred keV per nucleon for the energy-loss experiments at CEA-DIF, we have developed a different CVD-diamond detector based on a coplanar electrode geometry. In this alternative configuration, the electrodes are interdigitated and are both patterned on the same surface of the diamond film, while the other surface is not metallized. Then, the electric field remains close and nearly parallel to the diamond surface, which causes a charge transport parallel to the surface. Hence, the detection efficiency is optimized near the detector surface, which is well-suited to low-energy ions whose range is comparable to the field depth. A coplanar electrode geometry is all the more relevant for polycrystalline diamond when patterned on the growth surface as it restricts charge transport to the diamond region where the grains are largest in size.

The interdigitated electrode geometry has shown promising timing performances in the detection of α-particles[29–33] and it has also been successfully applied in the detection of UV and X-ray radiation as well as in charged-particle TOF spectroscopy[34–37]. In contrast to the sandwich configuration, the CCE and, thus, the pulse height response, is non-uniform accross the active diamond surface due to the non-uniform electric field profile. To a lesser extent, pulse amplitudes are also influenced by charge-trapping effects due to the polycrystalline nature of the diamond. However, in our experiments we consider bunch signals averaged over at least several hundred single-ion pulses.

The detector has been assembled and characterized at CEA-LIST. Its layout and electrical circuit are presented in Fig. 1. The diamond is a free-standing optical-grade polycrystalline film supplied by Diamond Materials[38]. It has a total area of 23×23 mm^2 and a thickness of 300 µm. The electrode fingers are made of a 200 nm thick aluminium layer. They were patterned using a standard photolithography technique on the diamond growth surface, where the grain size is estimated to

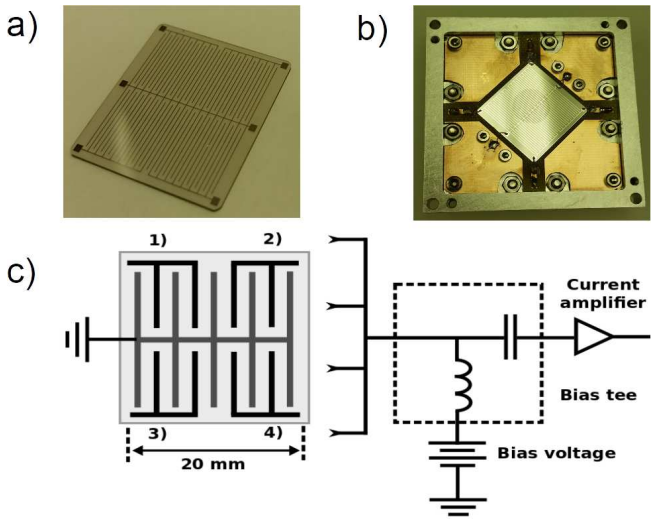

FIG. 1: a) Picture of the diamond film with its electrode pattern. b) Picture of the assembled detector. c) Scheme of the electrode pattern, made of four distinct segments, and of the circuit for signal transmission.

be around 60 µm. The electrodes have a finger width of 100 µm and a spacing of 500 µm. The active detector area is 20×20 mm^2, which was chosen according to beam transport simulations using the Monte-Carlo toolkit GEANT4[39,40]. Such area indeed guarantees the detection of at least few hundred ions per bunch for the experimental beam and target parameters described below (see Fig. 5). In order to minimize the capacitance value and thus the signal width, the electrode pattern is split in four equal segments of 10×10 mm^2. According to the model by Olthuis et al.[41], each segment features a capacitance value of 6.2 pF. Combined with the 50 Ω impedance of the signal transmission line, this leads to a detector decay time of 315 ps. This short time response, combined with the expected experimental bunch width of 1–2 ns at full width at half maximum (FWHM), provides access to narrow signals and therefore a high TOF resolution. The metallized diamond substrate was fixed on its printed circuit board (PCB) using araldite glue. The contacts of the electrode segments and of the ground were bonded to the PCB tracks with silver loaded resin. Finally, the device was mounted within an aluminium housing.

The current-voltage curve of the detector, measured under vacuum, is displayed in Fig. 2 for the four segments and for voltage values between -400 V and +400 V. As is shown, the leakage current has negligible values smaller than 150 pA. The detector was characterized in terms of transient current signals and of CCE distribution using α-particles at 5.486 MeV energy from an uncollimated 4 kBq ^{241}Am radioactive source, located at a distance of 10 mm from the detector surface. The measurements were carried out in air, as tests in air and in vacuum turned out to deliver very similar results. The data were

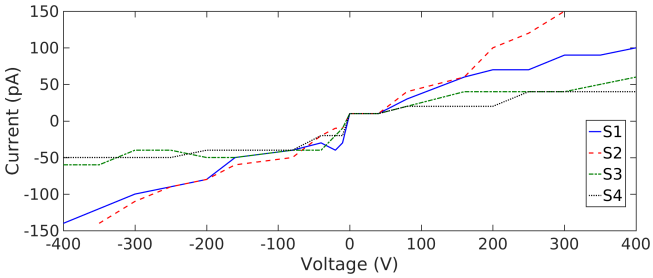

FIG. 2: I-V curve for the four detector segments measured under vacuum.

registered on a digital oscilloscope with an analog bandwidth of 2.5 GHz and a sampling rate of 40 GS/s. The transient current signals, as all current measurements reported in this work, have been obtained after amplification using a Cividec C2 low-noise 2 GHz broadband amplifier[42] with a gain of 40 dB. The CCE spectrum is directly obtained from the time integration of the transient current signals. A detection threshold of 20 mV was used, which enabled to capture all single α-particle events just above the noise. The data have been acquired for detector bias voltages of -300 V and +300 V, respectively. The measurements of the transient current signals are presented in Fig. 3 for each detector segment, while the obtained CCE spectra are displayed in Fig. 4a. Since the CCE results are very similar for all detector segments, data are only shown for one segment (S1).

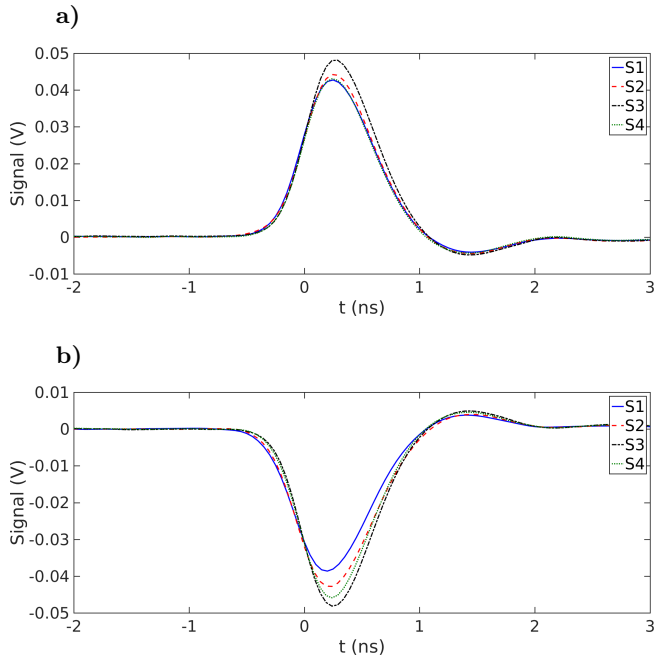

FIG. 3: Measured transient current signals averaged over one thousand single α-particle events at 5.486 MeV energy for the four detector segments (S1–S4), for an applied bias voltage of -300 V (a)) and +300 V (b)).

The CCE spectrum of a parallel-plate detector made of single-crystal electronic grade CVD diamond, measured to reach a nearly 100 % efficiency, is used as a reference measurement. In correspondence with the broad CCE spectrum of Fig. 4a, single transient current signals can feature large amplitude and shape variations. This is why here, each displayed transient current signal is an average over one thousand acquisitions. For both bias values the mean signal amplitudes reach around 40–50 mV and the amplitude differences between the various detector segments remain smaller than 20 %. The detector decay time is determined by fitting the signals with an exponentially modified Gaussian function. Respective values of 374, 360, 316 and 337 ps are found for the four segments with errors around 10 %, which is slightly above the theoretical prediction. The signal rise time, which corresponds to the root mean square of the detector decay time and of the amplifier rise time of 180 ps, is around 400 ps. The transient current signal width at FWHM turns out to be close to 700 ps, which demonstrates the short detector time response. As for the CCE spectra, the maximum CCE values reach around 20–25 % and the average CCE values are similar for both bias polarities, being 6.5 % and 5.0 % for +300 V and -300 V voltages, respectively. These values correspond to respective mean collected charges of 28 pC and 21 pC. The stability of

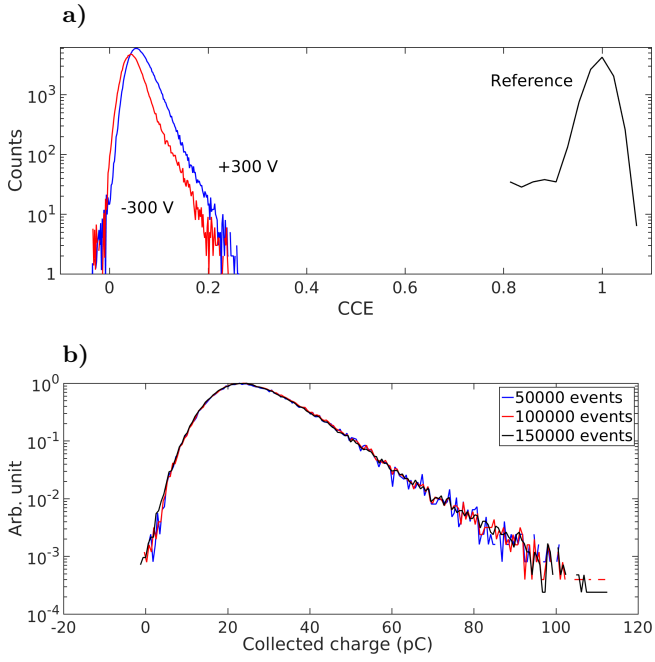

FIG. 4: a): charge collection efficiency (CCE) spectrum for one detector segment (S1) and bias voltages of -300 V and +300 V, normalized to a reference spectrum obtained with a 100 % CCE single crystal CVD diamond detector. b): normalized charge collection spectrum measured after 50000, 100000 and 150000 events, corresponding to roughly 5, 10 and 15 hours of irradiation with the α-particle source.

the charge collection process over time is illustrated in Fig. 4b, showing the measured charge collection spectrum after irradiation times of approximately 5, 10 and 15 hours which correspond to 50000, 100000 and 150000 detected events respectively. These data demonstrate that there is no degradation of the charge collection over time due to polarization in diamond. Due to the slightly higher efficiency using the positive bias configuration, the detector is always operated with a bias voltage of +300 V in the following.

It can be noted that due to the broad CCE spectrum and the relatively low average CCE value, measurements with the detector require sufficient ion statistics for obtaining exploitable signals as well as for reaching the reported timing properties. This is why the detector is only suited for measurements implying a sufficient statistical sample of events, e.g. using ion bunches with hundreds or thousands of particles. But it is not necessarily appropriate for measurements with single ionizing particles, that may induce strongly varying signal amplitudes and timing characteristics depending on the position where they impinge on the detector. It should also be noted that the 5.486 MeV energy α-particles used for the detector characterization have a range in diamond of around 13 µm, as can be estimated using the SRIM stopping database[43]. As α-particles for the energies of interest of few hundred keV per nucleon have a range of only a few micrometers in diamond, transient signals as well as CCE spectra are likely to differ for these projectiles.

The detector has been tested at the 4MV accelerator facility of CEA-DIF, where proton and α-particle beams in the 0.5–4 MeV energy range can be generated. We used α-particles at 500 keV per nucleon energy (total energy $E = 2$ MeV) as projectiles. The beam was bunched with a 5 µs period using a newly implemented field-programmable gate array. The beam current was of few hundred nA, which resulted in an ion fluence on the detector of around 5×10^6 cm^{-2} s^{-1}. In a laser-induced plasma, the target conditions vary significantly over a nanosecond time scale. Therefore the bunches, of originally 10–15 ns width, are shortened to 1–2 ns at FWHM with a Mobley compression system[44]. The beam energy resolution from the accelerator source is of the order of $\delta E/E \approx 10^{-3}$. In the beam-plasma experiments, the ion energy loss in the target is determined by comparing the TOF of the bunches that interact with the solid target or with the plasma and those that propagate in vacuum.

Here, we evaluate the detector TOF resolution by measuring the bunch signals after propagation in vacuum. Then, we present an example of TOF measurement after an approximately 2 m distance following the ion interaction with a carbon foil of 100 ± 1 µg/cm^2 thickness and 1.3 g/cm^3 density. According to the GEANT4 simulations, the ion energy loss in this target is $\Delta E = 143.9$ keV, with a straggling in energy at 1σ of 7.0 keV. It can be noted that the energy loss of 2 MeV energy α-particles in the aluminium electrode of 200 nm is estimated to be 54 keV, i.e. 2.7 % of the beam energy, which has a negligible effect on the projectile range in diamond and thus on the collected signals. In the beam measurements reported here, the signals are obtained by summing the contributions from the four detector segments before fast amplification, which means that the capacitance value in this case is not yet minimized. The data aquisition is carried out on a digital oscilloscope with a 8 GHz analog bandwidth in several series of 200 µs (40 bunches) in order to keep an optimal sampling period of 25 ps. The experimental setup is presented in Fig. 5. No beam refocusing after the target is employed but two pinholes can be used for beam collimation as is discussed later on. As mentioned before, each bunch impinging on the detector contains several hundred ions according to the GEANT4 simulations. Bunch signals in vacuum have, in average, a width of 1.4 ns at FWHM owing to the Mobley compression and to the fast detector response. Meanwhile, bunch signals after interaction with the carbon target have a larger width around 1.9 ns at FWHM, which is in agreement with the simulated energy straggling value. Note that the signals will be even shorter in future experiments when minimizing the decay time by using one amplifier per segment. Examples of bunch signals, both in vacuum and after the target, each averaged over one single measurement series of 40 bunches, are presented in Fig. 6. One of the single-particle signals

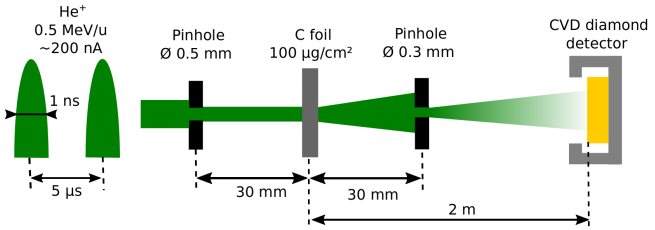

FIG. 5: Setup for the test of the detector on the 4 MV accelerator facility.

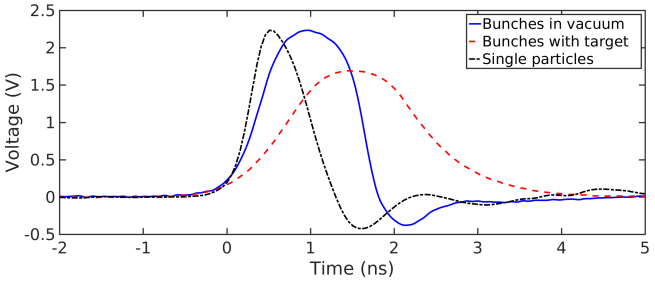

FIG. 6: Detector signals for a 500 keV per nucleon energy ($E = 2$ MeV) α-particle bunch in vacuum and after interaction with the target, each averaged over 40 bunches. A single α-particle signal at $E = 5.486$ MeV energy, taken from Fig. 3 and scaled for clarity, is shown for comparison. The signals, acquired at a bias voltage of +300 V, have been inverted to be displayed as positive.

shown in Fig. 3 is also plotted for comparison, its amplitude being normalized to the one of the shown bunch signal in vacuum. The signal amplitude with the target tends to be lower due to the angular straggling but no strict comparison can be done due both to possible fluctuations of the source and to the spatially non-uniform detector pulse height response.

The analysis of the bunch signals in vacuum gives an estimation of the optimum detector resolution. On the other hand, bunch signals after the target are convoluted with the straggling functions specific to the considered target, which leads to a degraded measurement resolution. For the considered TOF measurement using ion bunches, the TOF resolution is defined as the fluctuation of the measured bunch period. As the TOF of one bunch is given by its signal center of mass, the TOF resolution δt is evaluated using the 1σ fluctuation of the centers of mass of two consecutive bunch signals t_i and t_{i+1}. The distributions of the measured $t_{i+1} - t_i$ are displayed in Fig. 7 for 200 bunch signals coming from 5 distinct measurement series of 40 bunches each. All the data discussed in the following are averaged over these measured 200 bunches. Fitting the distributions of $t_{i+1} - t_i$ with Gaussian functions, the TOF resolution is determined as $\delta t = \sigma(t_{i+1} - t_i)/\sqrt{2}$. The energy resolution δE is deduced knowing the projectile energy E, its velocity v and the TOF distance d, using the relation $\delta E/E = 2\,\delta t\, v/d$. For the bunches propagating in vacuum (Fig. 7a), we obtain a TOF resolution $\delta t_{\rm vac} = 20\,$ps, which gives an estimate of the intrinsic time resolution of the detector. This value corresponds to an excellent energy resolution $\delta E_{\rm vac} = 0.4\,$keV of the ions at the target position, which represents 0.02 % of the projectile energy E. This value is better than the energy resolution from the accelerator because only a limited interval of ion energies is detected due to the enhanced beam divergence with the Mobley compression, together with the small detector solid angle. On the other hand, the TOF resolution obtained with the carbon target (Fig. 7b) is approximately $\delta t_{\rm tar} = 40\,$ps, which corresponds to $\delta E_{\rm tar} = 0.7\,$keV. Hence, the degradation of the resolution due to the straggling is moderate and we still resolve about 0.04 % of the ion energy. Consequently, we obtain an excellent resolution on the ion energy loss ΔE in the solid target of $\delta_{\Delta E} = \sqrt{\delta E_{\rm vac}^2 + \delta E_{\rm tar}^2} \approx 0.8\,$keV, or 0.6 % of ΔE. The data are summarized in Table I. In the energy-loss experiments with the plasma, the beam collimation is necessary due to the small diameter of the laser focal spot on the target of 0.5 mm compared to the diameter of the incoming ion beam of around 5 mm at FWHM. Therefore, one pinhole is required before the target position in order to guarantee quasi-monodimensional plasma conditions seen by interacting ions, and another pinhole is required after the target position for restricting the detector solid angle to the ions that have interacted with those uniform conditions. GEANT4 beam transport simulations accounting for the beam emittance allowed to find an optimum configuration with a 0.5 mm diameter pinhole located 30 mm in front of the target and another 0.3 mm diameter pinhole positioned 30 mm behind the target (see Fig. 5).

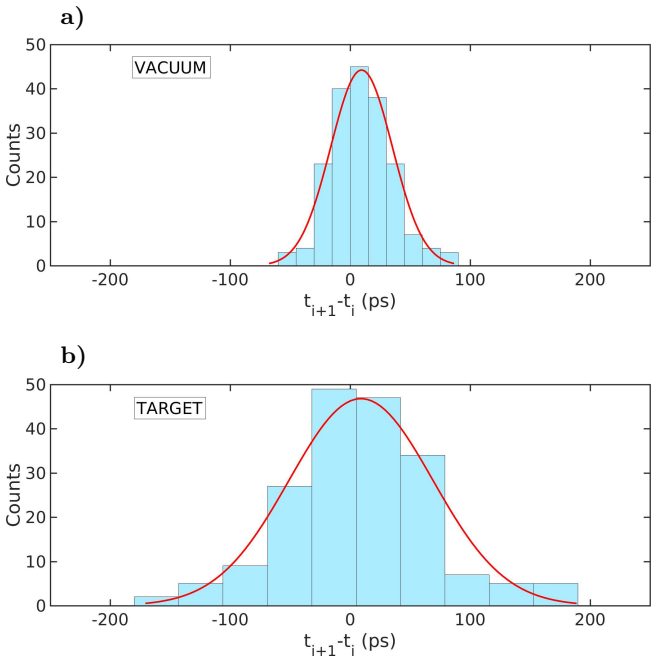

FIG. 7: Distribution of time differences $t_{i+1} - t_i$ between two consecutive ion bunches for a series of 200 bunches from 5 distinct measurement series. The data are shown for a propagation in vacuum (a)) and for a 2 m propagation after beam slowing down in the carbon target (b)). Each distribution is fitted with a Gaussian function for estimating the corresponding bunch TOF resolution.

A similar analysis of the detector signals is performed for the collimated beam and the results are also shown in Table I. The signal amplitude and width at FWHM are reduced due to collimation. The TOF and the energy resolutions obtained in vacuum are comparable to the ones found without collimation due to sufficient ion statistics. However, with the target the signal-to-noise ratio is significantly decreased owing to a 80 % smaller ion collection on the detector due to angular straggling as indicated by the GEANT4 results. Consequently, the TOF resolution is degraded to $\delta t_{\rm tar} = 150\,$ps, which leads to a resolution of $\delta E_{\rm tar} = 3.5\,$keV on the ion energy. This still corresponds to a highly precise measurement of 0.17 % of the ion energy and it leads to a resolution of $\delta_{\Delta E} = 3.6\,$keV or 2.5 % on the ion energy loss ΔE.

In conclusion, our detector permits an excellent TOF resolution down to 20 ps for α-particle bunches at 500 keV per nucleon energy. This is comparable to the resolutions reached with high-energy ions and a plane capacitor electrode geometry. The discrepancies of up to 30 % in the stopping-power predictions around the stopping-power peak in a laser-induced plasma[1] lead to energy-loss differences of at least several tens of keV for the considered carbon target. The energy-loss resolution of a few

No collimation	Amplitude	Width	δt	δE	δE/E	$\delta_{\Delta E}$	$\delta_{\Delta E}/\Delta$E
Vacuum	2.4 V	1.4 ns	20 ps	0.4 keV	0.02 %	-	-
Target	1.9 V	1.9 ns	40 ps	0.7 keV	0.04 %	0.8 keV	0.6 %
Collimation	Amplitude	Width	δt	δE	δE/E	$\delta_{\Delta E}$	$\delta_{\Delta E}/\Delta$E
Vacuum	0.3 V	0.9 ns	40 ps	0.8 keV	0.04 %	-	-
Target	0.09 V	1.8 ns	150 ps	3.5 keV	0.17 %	3.6 keV	2.5 %

TABLE I: Mean signal amplitude, width at FWHM as well as TOF (δt) and energy (δE) resolutions obtained for bunch measurements in vacuum and with a 100 µg/cm^2 thick carbon target and a 2 m TOF distance, as well as resolution on the measured energy loss in the target $\delta_{\Delta E}$. The data are presented without and with beam collimation respectively.

keV or less obtained from TOF measurements using our detector clearly enables to distinguish these differences experimentally and, thus, to benchmark the stopping-power models. Therefore the detector satisfies the requirements for the energy-loss experiments at CEA-DIF. It can be noted that a few studies report a worse radiation hardness of diamond compared to silicon for low-energy ions[26,45]. However, in our case possible polarization effects due to radiation damage are mitigated by the interdigitated structure. The absence of polarization effects can be noticed from the stability of the charge collection over time shown in Fig. 4b. This is also corroborated and reinforced by the fact that no signal degradation was observed in our experiments with ion bunches after a flux of 10^{10}–10^{11} ions cm^{-2} on the detector. In view of the non-uniform electric field profile due to the interdigitated structure and in particular in order to understand the relatively small measured CCE values, a more detailed characterization of the detector response will be performed. For this purpose, measurements using the Ion Beam Induced Charge (IBIC) method[46,47] as well as the Transient Current Technique (TCT)[48] for beam energies around 500 keV per nucleon are planned. In this way, the CCE and the temporal pulse response will be mapped accross the detector active surface for the exact projectile conditions of the experiment. This will enable us, with the help of simulations of the electric field, to optimize the electrode geometry and, thus, the measured bunch signals.

ACKNOWLEDGMENTS

We thank N. Skukan for the manufacturing of the detector printed circuit board in short time delays. We acknowledge B. Lommel and the staff of the Target Laboratory of GSI for producing the carbon foils used in the measurements. We thank the operating team of the 4MV accelerator as well as the dedicated mechanical workshop for their excellent support in the experiments.

[1] W. Cayzac, V. Bagnoud, M. M. Basko, A. Blažević, A. Frank, D. O. Gericke, L. Hallo, G. Malka, A. Ortner, A. Tauschwitz, J. Vorberger, and M. Roth, Phys. Rev. E **92**, 053109 (2015).
[2] C. Deutsch and G. Maynard, Matter and Radiation at Extremes **1**, 277 (2016).
[3] B. Y. Sharkov, D. H. Hoffmann, A. A. Golubev, and Y. Zhao, Matter and Radiation at Extremes **1**, 28 (2016).
[4] G. S. Fraley, E. J. Linnebur, R. J. Mason, and R. L. Morse, Physics of Fluids **17**, 474 (1974).
[5] R. L. Singleton, Physics of Plasmas **15**, 056302 (2008).
[6] M. Temporal, B. Canaud, W. Cayzac, R. Ramis, and R. L. Singleton, European Physical Journal D **71**, 132 (2017).
[7] P. A. Seidl, J. J. Barnard, A. Faltens, and A. Friedman, Physical Review Special Topics Accelerators and Beams **16**, 024701 (2013).
[8] J. C. Fernández, B. J. Albright, F. N. Beg, M. E. Foord, B. M. Hegelich, J. J. Honrubia, M. Roth, R. B. Stephens, and L. Yin, Nuclear Fusion **54**, 054006 (2014).
[9] J. A. Frenje, P. E. Grabowski, C. K. Li, F. H. Séguin, A. B. Zylstra, M. Gatu Johnson, R. D. Petrasso, V. Y. Glebov, and T. C. Sangster, Physical Review Letters **115**, 205001 (2015).
[10] W. Cayzac, A. Frank, A. Ortner, V. Bagnoud, M. M. Basko, S. Bedacht, C. Bläser, A. Blažević, S. Busold, O. Deppert, J. Ding, M. Ehret, P. Fiala, S. Frydrych, D. O. Gericke, L. Hallo, J. Helfrich, D. Jahn, E. Kjartansson, A. Knetsch, D. Kraus, G. Malka, N. W. Neumann, K. Pépitone, D. Pepler, S. Sander, G. Schaumann, T. Schlegel, N. Schroeter, D. Schumacher, M. Seibert, A. Tauschwitz, J. Vorberger, F. Wagner, S. Weih, Y. Zobus, and M. Roth, Nature Communications **8**, 15693 (2017).
[11] R. J. Tapper, Reports on Progress in Physics **63**, 1273 (2000).
[12] H. Pernegger, Physica Status Solidi Applied Research **203**, 3299 (2006).
[13] E. Berdermann, K. Blasche, P. Moritz, H. Stelzer, and B. Voss, Diamond and Related Materials **10**, 1770 (2001).
[14] M. Pomorski, E. Berdermann, A. Caragheorgheopol, M. Ciobanu, M. Kiš, A. Martemiyanov, C. Nebel, and P. Moritz, Physica Status Solidi Applied Research **203**, 3152 (2006).
[15] E. Berdermann, M. Pomorski, W. de Boer, M. Ciobanu, S. Dunst, C. Grah, M. Kiš, W. Koenig, W. Lange, W. Lohmann, R. Lovrinčić, P. Moritz, J. Morse, S. Mueller, A. Pucci, M. Schreck, S. Rahman, and M. Träger, Diamond and Related Materials **19**, 358 (2010).
[16] F. Schirru, B. S. N. Singh, L. Scruton, M. A. Bentley, S. P. Fox, A. Lohstroh, P. J. Sellin, A. Banu, M. McCleskey, B. T. Roeder, E. Simmons, A. A. Alharbi, L. Trache, M. Freer, and D. Parker, Journal of Instrumentation **7**, P05005 (2012).
[17] S. Michimasa, M. Takaki, M. Dozono, S. Go, H. Baba, E. Ideguchi, K. Kisamori, H. Matsubara, H. Miya, S. Ota, H. Sakai, S. Shimoura, A. Stolz, T. L. Tang, H. Tokieda, T. Uesaka, and R. G. T. Zegers, Nuclear Instruments and Methods in Physics Research B **317**, 710 (2013).
[18] W. Trischuk, M. Artuso, F. Bachmair, L. Bäni, M. Bartosik, V. Bellini, V. Belyaev, B. Bentele, E. Berdermann, P. Bergonzo, A. Bes, J.-M. Brom, M. Bruzzi, M. Cerv, C. Chau, G. Chiodini, D. Chren, V. Cindro, G. Claus, J. Collot, S. Costa, J. Cumalat, A. Dabrowski, R. D'Alessandro, W. de Boer, B. Dehning, D. Dobos, W. Dulinski, V. Eremin, R. Eusebi, G. Forcolin,

J. Forneris, H. Frais-Kölbl, K. K. Gan, M. Gastal, M. Goffe, J. Goldstein, A. Golubev, L. Gonella, A. Gorišek, L. Graber, E. Grigoriev, J. Grosse-Knetter, M. Guthoff, I. Haughton, D. Hidas, D. Hits, M. Hoeferkamp, T. Hofmann, J. Hosslet, J.-Y. Hostachy, F. Hügging, H. Jansen, J. Janssen, H. Kagan, K. Kanxheri, G. Kasieczka, R. Kass, F. Kassel, M. Kis, G. Kramberger, S. Kuleshov, A. Lacoste, S. Lagomarsino, A. Lo Giudice, C. Maazouzi, I. Mandic, C. Manfredotti, C. Mathieu, N. McFadden, G. McGoldrick, M. Menichelli, M. Mikuž, A. Morozzi, J. Moss, R. Mountain, S. Murphy, A. Oh, P. Olivero, G. Parrini, D. Passeri, M. Pauluzzi, H. Pernegger, R. Perrino, F. Picollo, M. Pomorski, R. Potenza, A. Quadt, A. Re, G. Riley, S. Roe, M. Sapinski, M. Scaringella, S. Schnetzer, T. Schreiner, S. Sciortino, A. Scorzoni, S. Seidel, L. Servoli, A. Sfyrla, G. Shimchuk, S. Smith, B. Sopko, V. Sopko, S. Spagnolo, S. Spanier, K. Stenson, R. Stone, C. Sutera, A. Taylor, M. Traeger, D. Tromson, W. Trischuk, C. Tuve, L. Uplegger, J. Velthuis, N. Venturi, E. Vittone, S. Wagner, R. Wallny, J. C. Wang, P. Weilhammer, J. Weingarten, C. Weiss, T. Wengler, N. Wermes, M. Yamouni, M. Zavrtanik, and RD42 Collaboration, Nuclear and Particle Physics Proceedings **273**, 1023 (2016).

[19] M. Rebisz, B. Voss, A. Heinz, E. Usenko, and M. Pomorski, Diamond and Related Materials **16**, 1070 (2007).

[20] A. Frank, A. Blažević, P. L. Grande, K. Harres, T. Heßling, D. H. H. Hoffmann, R. Knobloch-Maas, P. G. Kuznetsov, F. Nürnberg, A. Pelka, G. Schaumann, G. Schiwietz, A. Schökel, M. Schollmeier, D. Schumacher, J. Schütrumpf, V. V. Vatulin, O. A. Vinokurov, and M. Roth, Physical Review E **81**, 026401 (2010).

[21] A. Frank, A. Blažević, V. Bagnoud, M. M. Basko, M. Börner, W. Cayzac, D. Kraus, T. Heßling, D. H. H. Hoffmann, A. Ortner, A. Otten, A. Pelka, D. Pepler, D. Schumacher, A. Tauschwitz, and M. Roth, Physical Review Letters **110**, 115001 (2013).

[22] W. Cayzac, A. Frank, D. Schumacher, M. Roth, A. Blažević, F. Wamers, M. Träger, E. Berdermann, B. Voss, and T. Hessling, Review of Scientific Instruments **84**, 043301 (2013).

[23] S. Han and R. S. Wagner, Applied Physics Letters **68**, 3016 (1996).

[24] D. M. Trucchi, E. Cappelli, G. Conte, G. Mattei, C. Gramaccioni, and P. Ascarelli, Diamond and Related Materials **14**, 575 (2005).

[25] C. Manfredotti, A. Lo Giudice, E. Vittone, F. Fizzotti, Y. Garino, and E. Pace, Diamond and Related Materials **15**, 1467 (2006).

[26] V. Grilj, N. Skukan, M. Jakšić, W. Kada, and T. Kamiya, Nuclear Instruments and Methods in Physics Research B **306**, 191 (2013).

[27] W. Kada, N. Iwamoto, T. Satoh, S. Onoda, V. Grilj, N. Skukan, M. Koka, T. Ohshima, M. Jakšić, and T. Kamiya, Nuclear Instruments and Methods in Physics Research B **331**, 113 (2014).

[28] Y. Sato, T. Shimaoka, J. H. Kaneko, H. Murakami, M. Isobe, M. Osakabe, M. Tsubota, K. Ochiai, A. Chayahara, H. Umezawa, and S. Shikata, Nuclear Instruments and Methods in Physics Research A **784**, 147 (2015).

[29] P. Bergonzo, F. Foulon, R. D. Marshall, C. Jany, A. Brambilla, R. D. McKeag, and R. B. Jackman, IEEE Transactions on Nuclear Science **45**, 370 (1998).

[30] P. J. Sellin and M. B. H. Breese, IEEE Transactions on Nuclear Science **48**, 2307 (2001).

[31] A. Galbiati, M. B. H. Breese, A. P. Knights, B. Sealy, and P. J. Sellin, Nuclear Instruments and Methods in Physics Research A **466**, 52 (2001).

[32] S. G. Wang, Q. Zhang, Q. Wang, S. F. Yoon, J. Ahn, Q. Zhou, D. J. Yang, and J. Q. Li, Diamond and Related Materials **12**, 682 (2003).

[33] L. Wang, Y. Lou, Q. Su, W. Shi, and Y. Xia, Optics Express **13**, 8612 (2005).

[34] R. D. McKeag, R. D. Marshall, B. Baral, S. S. M. Chan, and R. B. Jackman, Diamond and Related Materials **6**, 374 (1997).

[35] S. Almaviva, M. Marinelli, E. Milani, G. Prestopino, A. Tucciarone, C. Verona, G. Verona-Rinati, M. Angelone, and M. Pillon, Diamond and Related Materials **19**, 78 (2010).

[36] M. Marinelli, E. Milani, G. Prestopino, C. Verona, G. Verona-Rinati, M. Cutroneo, L. Torrisi, D. Margarone, A. Velyhan, J. Krasa, and E. Krousky, Applied Surface Science **272**, 104 (2013).

[37] R. De Angelis, F. Consoli, C. Verona, G. Di Giorgio, P. Andreoli, G. Cristofari, M. Cipriani, F. Ingenito, M. Marinelli, and G. Verona-Rinati, Journal of Instrumentation **11**, C12048 (2016).

[38] Diamond Materials GmbH, http://www.diamond-materials.com.

[39] S. Agostinelli, J. Allison, K. Amako, J. Apostolakis, H. Araujo, P. Arce, M. Asai, D. Axen, S. Banerjee, G. Barrand, F. Behner, L. Bellagamba, J. Boudreau, L. Broglia, A. Brunengo, H. Burkhardt, S. Chauvie, J. Chuma, R. Chytracek, G. Cooperman, G. Cosmo, P. Degtyarenko, A. Dell'Acqua, G. Depaola, D. Dietrich, R. Enami, A. Feliciello, C. Ferguson, H. Fesefeldt, G. Folger, F. Foppiano, A. Forti, S. Garelli, S. Giani, R. Giannitrapani, D. Gibin, J. G. Cadenas, I. González, G. G. Abril, G. Greeniaus, W. Greiner, V. Grichine, A. Grossheim, S. Guatelli, P. Gumplinger, R. Hamatsu, K. Hashimoto, H. Hasui, A. Heikkinen, A. Howard, V. Ivanchenko, A. Johnson, F. Jones, J. Kallenbach, N. Kanaya, M. Kawabata, Y. Kawabata, M. Kawaguti, S. Kelner, P. Kent, A. Kimura, T. Kodama, R. Kokoulin, M. Kossov, H. Kurashige, E. Lamanna, T. Lampén, V. Lara, V. Lefebure, F. Lei, M. Liendl, W. Lockman, F. Longo, S. Magni, M. Maire, E. Medernach, K. Minamimoto, P. M. de Freitas, Y. Morita, K. Murakami, M. Nagamatu, R. Nartallo, P. Nieminen, T. Nishimura, K. Ohtsubo, M. Okamura, S. O'Neale, Y. Oohata, K. Paech, J. Perl, A. Pfeiffer, M. Pia, F. Ranjard, A. Rybin, S. Sadilov, E. D. Salvo, G. Santin, T. Sasaki, N. Savvas, Y. Sawada, S. Scherer, S. Sei, V. Sirotenko, D. Smith, N. Starkov, H. Stoecker, J. Sulkimo, M. Takahata, S. Tanaka, E. Tcherniaev, E. S. Tehrani, M. Tropeano, P. Truscott, H. Uno, L. Urban, P. Urban, M. Verderi, A. Walkden, W. Wander, H. Weber, J. Wellisch, T. Wenaus, D. Williams, D. Wright, T. Yamada, H. Yoshida, and D. Zschiesche, Nuclear Instruments and Methods in Physics Research Section A: Accelerators, Spectrometers, Detectors and Associated Equipment **506**, 250 (2003).

[40] J. Allison, K. Amako, J. Apostolakis, H. Araujo, P. Arce, M. Asai, G. Barrand, R. Capra, S. Chauvie, R. Chytracek, P. Cirrone, G. Cooperman, G. Cosmo, G. Cuttone, G. Daquino, M. Donszelmann, M. Dressel, G. Folger, F. Foppiano, and H. Yoshida, IEEE Transactions on Nuclear Science **53**, 270 (2006).

[41] W. Olthuis, W. Streekstra, and P. Bergveld, Sensors and Actuators B: Chemical **24**, 252 (1995).

[42] CIVIDEC Instrumentation GmbH, http://www.cividec.at.

[43] J. F. Ziegler, J. P. Biersack, and U. Littmark, *The Stopping and Range of Ions in Matter*, edited by P. Press (1985).

[44] R. C. Mobley, Phys. Rev. **88**, 360 (1952).

[45] I. Zamboni, Ž. Pastuović, and M. Jakšić, Diamond and Related Materials **31**, 65 (2013).

[46] P. J. Sellin, M. B. H. Breese, A. P. Knights, L. C. Alves, R. S. Sussmann, and A. J. Whitehead, Applied Physics Letters **77**, 913 (2000).

[47] M. B. H. Breese, E. Vittone, G. Vizkelethy, and P. J. Sellin, Nuclear Instruments and Methods in Physics Research B **264**, 345 (2007).

[48] H. Schone, D. S. Walsh, F. W. Sexton, B. L. Doyle, P. E. Dodd, J. F. Aurand, R. S. Flores, and N. Wing, IEEE Transactions on Nuclear Science **45**, 2544 (1998).